analytical chemistry

pubs.acs.org/ac Article

In Situ Exsolution of Noble-Metal Nanoparticles on Perovskites as Enhanced Peroxidase Mimics for Bioanalysis

Xiaoqian Jiang,[‖] Xiaoyu Wang,[‖] Anqi Lin, and Hui Wei*

Cite This: *Anal. Chem.* 2021, 93, 5954−5962 Read Online

ACCESS | Metrics & More | Article Recommendations | Supporting Information

ABSTRACT: Various transition-metal oxide (TMO)-based nanomaterials have been explored as peroxidase mimics. However, the moderate peroxidase-like activity of TMOs limited their widespread use. Decorating highly active noble-metal nanozymes on the surface of TMOs can not only enhance the peroxidase-like activity of TMOs but also prevent the small-sized metal nanoparticles (NPs) from aggregation. Herein, *in situ* exsolution of noble-metal NPs (i.e., Ir and Ru) from A-site-deficient perovskite oxides (i.e., chemical formula $La_{0.9}B_{0.9}B'_{0.1}O_{3-\delta}$, B = Mn/Fe, B′ = Ir/Ru) under a reducing atmosphere was achieved for preparing noble-metal NPs/perovskite composites. The exsolved NPs were socketed on the surface of parent perovskite oxides, which significantly enhanced the stability of metal NPs. In addition, the peroxidase-like activity of perovskite oxides increased remarkably after NPs egress. We then used the optimized Ir/LMIO with high stability and excellent peroxidase-like activity to develop a colorimetric assay for the determination of alkaline phosphatase (ALP). Benefiting from the remarkable peroxidase-like activity of Ir/LMIO, the sensing platform exhibited a wide linear range. The practical application of the colorimetric sensing method was demonstrated by detecting the ALP in serum samples. This work not only provides new insights into the synthesis of highly active peroxidase-like nanozymes but expands their applications for constructing a high-performance biosensing platform.

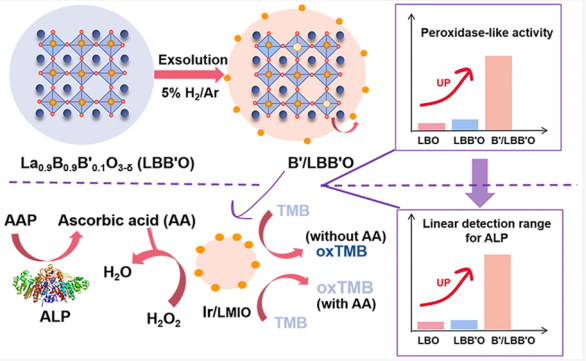

INTRODUCTION

Nanozymes are nanomaterials with enzyme-like catalytic activities.[1,2] Various types of enzymes such as oxidase, peroxidase, catalase, superoxide dismutase, and hydrolase have been mimicked using different kinds of nanomaterials.[3−7] Among these nanozymes, nanomaterials with peroxidase-like activity have received great attention due to their great promise in biosensing, bioimaging, and nanomedicine.[8−13] Yan and co-workers first discovered that Fe_3O_4 nanoparticles (NPs) could mimic a peroxidase that were then used as alternatives to horseradish peroxidase for immunoassays.[14] Inspired by this research, various transition-metal oxides (TMOs) were explored as peroxidase mimics.[15−18] However, most of the metal oxides nanozymes have moderate catalytic activity. Therefore, efficient strategies are needed to design highly active TMO-based peroxidase mimics. We have recently demonstrated that ABO_3-type perovskite oxides (where A is a rare-earth or alkaline-earth metal and B is a transition metal) are good candidates for this purpose due to their unique physical and chemical properties, flexible structures, and adjustable components.[19−22] We showed that the e_g occupancy is a predictive descriptor for the rational design of perovskite oxide-based nanozymes. $LaNiO_{3-\delta}$, optimized based on the e_g occupancy, possessed a peroxidase-like activity 1−2 orders of magnitude higher than that of other representative carbon-based and metal oxide-based nanozymes.[19] Even so, the peroxidase-like activity of perovskite oxides was still inferior to noble-metal-based nanozymes.

Previous studies demonstrated that metal NPs (e.g., Ru and Ir) with small sizes exhibited excellent peroxidase-like activity.[23,24] These noble-metal-based nanozymes were usually synthesized by a wet chemical reduction process.[24,25] To control the size and morphology of metal nanozymes, capping or encapsulating agents were employed during the synthesis. However, the capping agents on metal NP surface may block access to the catalytic sites, resulting in the decreased peroxidase-like activity. In addition, despite the presence of capping agents, metal-based nanozymes with small sizes could easily aggregate during practical catalysis process.

Recently, the exsolution based on *in situ* growth of metal NPs from a parent perovskite has been demonstrated as an effective method for preparing metal NPs/perovskite oxide composites.[26−29] The target transition metal (B′) was first incorporated into the lattice of A-site deficiency perovskite

Received: February 17, 2021
Accepted: March 23, 2021
Published: April 2, 2021

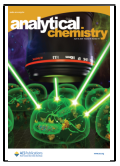

oxide to form $A_{1-x}B_{1-y}B'_yO_{3-\delta}$. Subsequently, the target transition metal (B′) was exsolved to form finely dispersed metal NPs under a reducing atomsphere.[30−33] Therefore, we envision that *in situ* exsolution of metal NPs on perovskites will not only improve the peroxidase-like activity of perovskite oxides but also prevent metal NPs from aggregation during the catalytic process.

Here, we proposed a strategy involving *in situ* exsolution of Ir or Ru NPs on the surface of perovskite oxides by A-site defects as driving forces under a reducing atmosphere. $La_{0.9}Mn_{0.9}Ir_{0.1}O_{3-\delta}$ (LMIO), $La_{0.9}Mn_{0.9}Ru_{0.1}O_{3-\delta}$ (LMRO), $La_{0.9}Fe_{0.9}Ir_{0.1}O_{3-\delta}$ (LFIO), and $La_{0.9}Fe_{0.9}Ru_{0.1}O_{3-\delta}$ (LFRO) were used as parent materials to *in situ* exsolve Ir or Ru NPs on perovskite oxides surface to form Ir/LMIO, Ru/LMRO, Ir/LFIO, and Ru/LFRO, respectively. $LaMnO_3$ was first chosen as the parent material due to its relatively good peroxidase-like activity and stability. Furthermore, to prove the universality of this method, $LaFeO_3$ was also used as a parent material for *in situ* exsolution of Ru and Ir NPs. The peroxidase-mimicking activity of Ir/LMIO, Ru/LMRO, Ir/LFIO, and Ru/LFRO exhibited about 10, 7, 50, and 30 times higher than their corresponding parent perovskite oxides.

Finally, Ir/LMIO with the highest peroxidase-like activity was employed to develop a reliable bioanalysis platform for the determination of alkaline phosphatase (ALP). ALP is present in the body fluids and tissues of human, which is a crucial diagnostic indicator of many diseases. Its abnormal level is mainly related to liver disease, biliary obstruction, metabolic disease, scurvy, bone diseases, etc.[34−36] The hydrolysis of phosphoryl esters could be catalyzed by ALP to produce ascorbic acid (AA),[37,38] which exhibited a competitive effect on the reaction between H_2O_2 and TMB. Based on this, we have built a colorimetric sensing platform to evaluate the ALP activity. Benefiting from the remarkable peroxidase-like activity of Ir/LMIO, the colorimetric method exhibited a wide linear range and a low detection limit.

EXPERIMENTAL SECTION

Chemicals and Materials. Lanthanum nitrate ($La(NO_3)_3\cdot 6H_2O$), iron nitrate ($Fe(NO_3)_3\cdot 9H_2O$), iridium chloride hydrate ($IrCl_3\cdot xH_2O$), ruthenium chloride hydrate ($RuCl_3\cdot xH_2O$), 3,3′,5,5′-tetramethylbenzidine (TMB), trypsin, glycine, glutamic acid, sarcosine, and glucose oxidase (GOx) were purchased from Aladdin Chemical Reagent Co., Ltd. Manganese nitrate ($Mn(NO_3)_2\cdot 4H_2O$) was obtained from Beijing Inokai Technology Co., Ltd. Hydrogen peroxide (H_2O_2), ethylene glycol, ascorbic acid (AA), and citric acid were purchased from Sinopharm Chemical Reagent Co., Ltd. Glucose was purchased from Nanjing Chemical Reagent Co., Ltd. Fructose was purchased from Shandong Xiya Reagent Co., Ltd. Ascorbic acid 2-phosphate (AAP), alkaline phosphatase (ALP), lysozyme, and bovine serum albumin (BSA) were purchased from Sigma-Aldrich. Human serum albumin (HSA) and lactate oxidase (LOx) were purchased from Shanghai Yuanye Bio-Technology Co., Ltd. All aqueous solutions used in the experiments were prepared with deionized water (18.2 MΩ·cm, Millipore).

Catalyst Preparations. The pristine perovskites were synthesized via a sol−gel method.[19] The respective stoichiometric metal nitrates (3 mmol in total) and citric acid (12 mmol) were dissolved in 100 mL of H_2O, then 1.5 mL of ethylene glycol was added under stirring. The resulting transparent solutions were treated at 90 °C with sufficient stirring and then evaporated to form gel. The gel was further heated at 180 °C for 5 h to form the solid precursors. The obtained solid precursor was decomposed at 400 °C for 2 h to remove the organic components and to obtain foam precursors. The foam precursors were further annealed in air at 900 °C for 5 h with a ramp rate of 5 °C/min to obtain the pristine perovskite (denoted as LMIO, LMRO, LFIO, and LFRO) and control samples ($LaMnO_3$ and $LaFeO_3$), respectively. Then, the pristine perovskite powders were reduced at 650 °C for 5 h in 5% H_2/Ar to obtain the final samples, namely, Ir/LMIO, Ru/LMRO, Ir/LFIO, and Ru/LFRO.

Instrumentation. Transmission electron microscopy (TEM) images were recorded on a JEOL JEM-2100 transmission electron microscope (JEOL, Japan) at an acceleration voltage of 200 kV. High-resolution transmission electron microscopy (HRTEM), high-angle annular dark-field scanning TEM (HAADF-STEM), and the corresponding energy-dispersive spectroscopy (EDS) elemental mappings were performed on an FEI Titan[33] G2 60-300 TEM equipped with an acceleration voltage of 300 kV and an EDS detector, respectively. Powder X-ray diffraction (XRD) patterns were obtained on a Rigaku Ultima X-ray diffractometer using Cu Kα radiation. X-ray photoelectron spectra (XPS) were collected using a PHI 5000 VersaProbe (Ulvac-Phi, Japan). UV−visible absorption spectra were collected using a spectrophotometer (TU-1900, Beijing Purkinje General Instrument Co. Ltd., China). The absorption in a 96-well plate at 652 nm was recorded by a SpectraMax M2e microplate reader (Molecular Devices).

Peroxidase-like Activity Measurements. The peroxidase-like activity was measured using TMB as a substrate. Steady-state kinetics assays were conducted at 25 °C in a 96-well plate and recorded in a microplate reader. For the kinetics assays of nanozymes, acetic acid−sodium acetate buffer (pH 4.5, 0.2 M) was used as the reaction buffer and 10 μg/mL of nanozymes were used. Kinetics data were obtained by changing the concentration of one substrate (i.e., H_2O_2 or TMB) and keeping that of the other constant. The absorption at 652 nm within 5 min was monitored continuously. The kinetics parameters (i.e., v_{max} and K_m) were calculated by fitting the reaction velocity values and the substrate concentrations to the Michaelis−Menten equation as follows

$$v = \frac{v_{max}[S]}{K_m + [S]} \quad (1)$$

where v is the initial reaction velocity, v_{max} is the maximal reaction velocity, K_m is the Michaelis constant, and $[S]$ is the substrate concentration.

Effect of AA on the Peroxidase-like Activity of Ir/LMIO. H_2O_2 (20 mM), TMB (500 μM), Ir/LMIO (2 μg/mL), and AA with various concentrations (0−200 μM) in 0.2 M acetic acid−sodium acetate buffer (pH 4.5) were mixed. Then, 100 μL of the reaction solution was added into a 96-well plate and the absorption at 652 nm was recorded in a microplate reader for 10 min at 25 °C.

Colorimetric Detection of ALP. Colorimetric ALP activity assay was performed as follows. First, 0.2 M Tris-HCl (pH 8.0), AAP (0.2 mM), and ALP (with different activities ranging from 0 to 200 U/L) were mixed and incubated in a 37 °C water bath for 40 min. Then, 0.2 M acetic acid−sodium acetate buffer (pH 4.5) was added to stop the

https://doi.org/10.1021/acs.analchem.1c00721
Anal. Chem. 2021, 93, 5954−5962

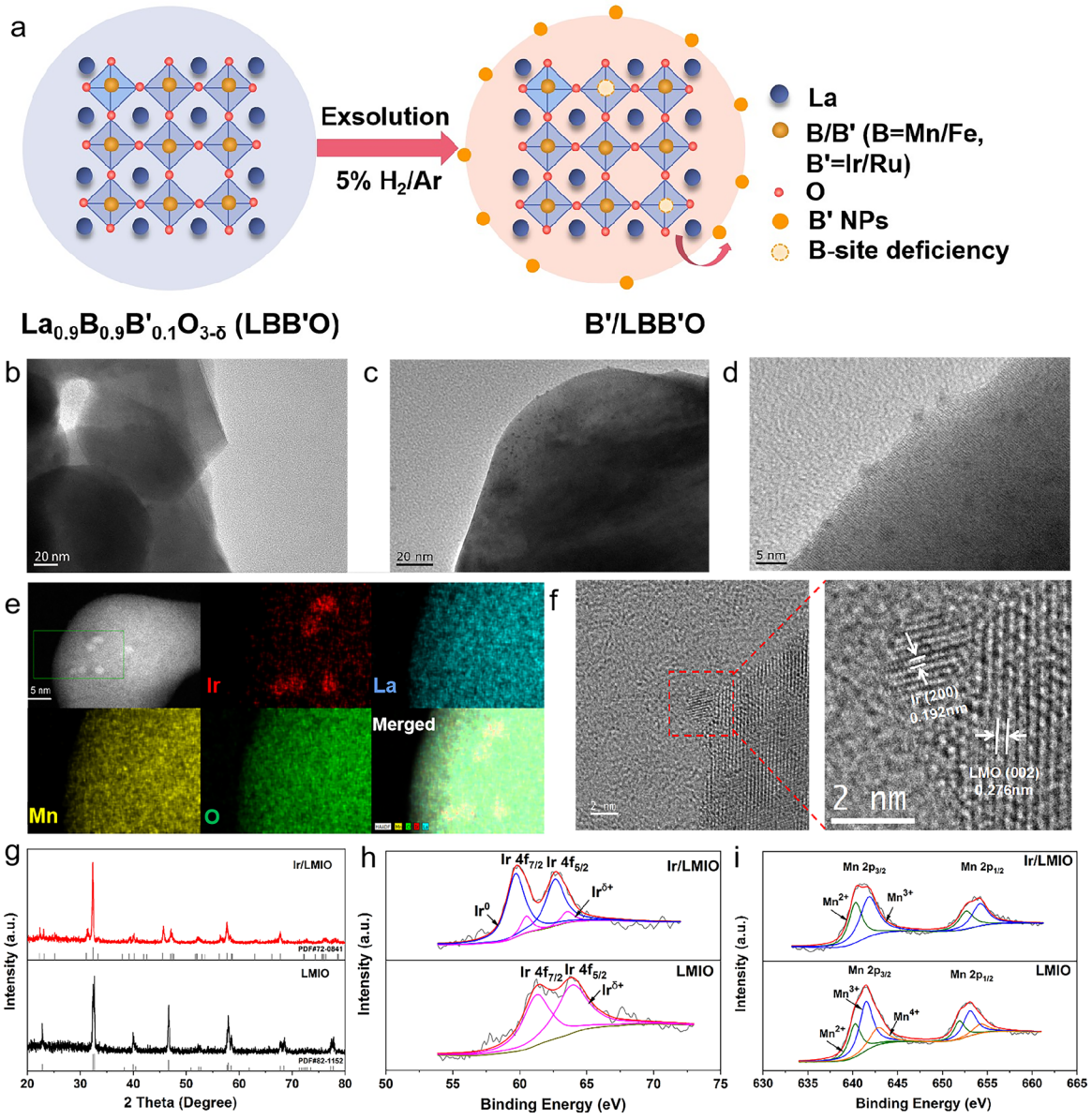

Figure 1. (a) Schematic illustration of the synthesis process of *in situ* exsolution of noble-metal NPs on perovskite. (b) TEM image of LMIO. (c, d) TEM images of Ir/LMIO. (e) HAADF-STEM image and EDS elemental mapping of Ir/LMIO. (f) HRTEM images of Ir/LMIO. (g) XRD patterns of LMIO and Ir/LMIO. (h, i) XPS profiles of LMIO and Ir/LMIO in Ir 4f spectrum and Mn 2p spectrum, respectively.

catalytic reaction. Subsequently, 2 μg/mL of Ir/LMIO (or LMIO and $LaMnO_3$), 0.5 mM TMB, and 90 mM H_2O_2 were added into the reaction solution. Then, 100 μL of the reaction solution was added into the 96-well plate and the absorption at 652 nm was recorded in a microplate reader for 10 min at 25 °C.

To investigate the selectivity of ALP detection, 100 U/L GOx, lysozyme, trypsin, and LOx, 500 μM metal ions (K^+, Na^+, and Ca^{2+}), 100 μM amino acids (glycine, glutamic acid, and sarcosine), fructose, glucose, 3 μM HSA, and BSA as interference were determined.

To detect ALP activity in serum samples, 25 μL of serum (5%) was spiked with different concentrations of ALP solution and diluted to 500 μL using 0.2 M Tris-HCl buffer (pH 8.0). Then, 0.2 mM AAP was added into the spiked samples as described above. After incubation at 37 °C for 40 min, the mixture was ultrafiltered to remove the interference with a Microcon centrifugal filter device (Ultracel YM-30 membrane, Millipore) for 3 min at 14 000 rpm. Finally, 100 μL of the above solution, 0.5 mM TMB, and 90 mM H_2O_2 were added into 0.2 M acetic acid−sodium acetate buffer (pH 4.5) (final total volume was 1 mL). Then, 100 μL of the reaction solution was added into a 96-well plate and the absorption at 652 nm was recorded in a microplate reader for 10 min at 25 °C.

RESULTS AND DISCUSSION

Synthesis and Characterization of the Perovskite-Based Nanozymes. *In situ* exsolution of Ir or Ru NPs on the surface of perovskite oxides was achieved by A-site defects as driving forces under a reducing atmosphere (Figure 1a). $LaMnO_3$ perovskite was first selected as the parent materials because it not only possesses excellent peroxidase-like activity but is stable upon annealing at a reducing atmosphere. To *in situ* exsolve Ir nanoparticle, $La_{0.9}Mn_{0.9}Ir_{0.1}O_{3-\delta}$ (LMIO) perovskite with A-site deficiency was synthesized, because A-

https://doi.org/10.1021/acs.analchem.1c00721
Anal. Chem. 2021, 93, 5954−5962

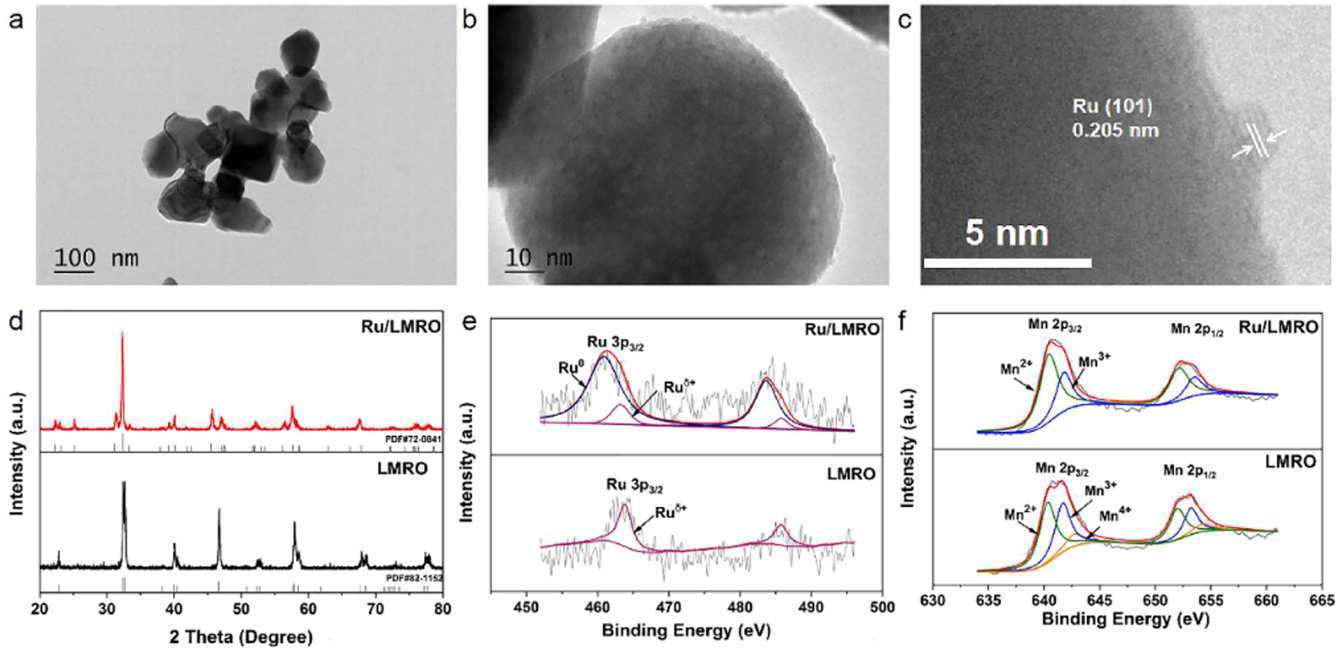

Figure 2. (a) TEM image of LMRO. (b, c) TEM images of Ru/LMRO. (d) XRD patterns of LMRO and Ru/LMRO. (e, f) XPS profiles of LMRO and Ru/LMRO in Ru 3p spectrum and Mn 2p spectrum, respectively.

site deficiency could serve as a driving force to trigger B-site egress.[30,39] As shown in Figure 1b, LMIO prepared by a sol−gel method exhibited a clean and smooth surface. However, many finely dispersed NPs with diameters of 1−2 nm were socketed on the surface of perovskite host after annealing LMIO at a reducing atmosphere (Figure 1c,d). To decipher the composition of the exsolved NPs, HAADF-STEM images coupled with EDS element mapping were performed. As presented in Figure 1e, after NPs exsolution, the uniform distribution of La, Mn, and O in the parent perovskite was observed. Most of surface Ir cations were reduced and became NPs, while the concentration of ionic Ir near the surface of the perovskite was negligible (Figure 1e). The HRTEM results in Figure 1f exhibited a magnified NP and perovskite matrix with well-defined lattice fringes. The NP with a *d*-spacing of 0.192 nm corresponded to cubic (space group *Fm*3*m*) Ir NPs indexed at the (200) crystal planes, while the perovskite matrix with a *d*-spacing of 0.276 nm corresponded to orthorhombic (space group *Pnma*) $LaMnO_3$ matrix indexed at the (002) crystal planes. Moreover, powder X-ray diffraction (XRD) was used to analyze the structure changes after NPs exsolution. Before annealing at 5% H_2/Ar, LMIO presented typical diffraction peaks of rhombohedral (JCPDS 82-1152) with a space group of *R*3*c*. No obvious impurities were observed, suggesting that Ir was successfully doped into the $LaMnO_3$ perovskite lattice. After reduction, the perovskite oxide was subjected to a structural phase change (Figure 1g).[31] The XRD patterns of LMIO and Ir/LMIO suggested that the lattice's structure transformed from rhombohedral (JCPDS 82-1152) to orthorhombic (JCPDS 72-0841) with a space group of *Pnma*. No new peaks from byproducts appeared after reducing. The peaks of Ir NPs were not observed in the XRD pattern, which may be attributed to the fact that the size of Ir NPs was too small to be detected by XRD. We further analyzed the chemical valence states of the nanozymes by X-ray photoelectron spectroscopy (XPS) measurements. As shown in Figure 1h, for the pristine LMIO, the binding energy of the Ir $4f_{7/2}$ was ∼61.26 eV, which belonged to $Ir^{\delta+}$, and no metallic Ir was detected. After treatment at 650 °C under a forming gas of 5% H_2 in argon, the Ir $4f_{7/2}$ was deconvoluted into two double peaks that can be assigned to Ir^0 and $Ir^{\delta+}$, with binding energies of 59.68 and 60.49 eV, respectively, indicating that Ir NPs have appeared on the surface of the perovskite matrix.[40] The average valence state of Mn decreased slightly after exsolution (Figure 1i).[31] The above results demonstrated that *in situ* exsolution of NPs from the parent perovskite could be an effective approach for synthesizing Ir NPs/perovskite composites.

To demonstrate the universality of *in situ* exsolution of noble-metal NPs from parental perovskites, Ru was taken as an another example due to its excellent peroxidase-like activity.[24] As shown in Figure 2a−c, metal NPs were embedded on the surface of the perovskites when the $La_{0.9}Mn_{0.9}Ru_{0.1}O_{3-\delta}$ (LMRO) was reduced at 5% H_2/Ar. In addition, HRTEM images confirmed that the NPs on the surface of perovskites with a *d*-spacing of 0.205 nm corresponded to Ru NPs (space group *P*63/*mmc*) indexed at the (101) crystal planes (Figure 2c). XRD results suggested that no other byproducts appeared after exsolution of Ru NPs (Figure 2d). The unique binding energy of the Ru $3p_{3/2}$ on LMRO was ∼463.83 eV, demonstrating that only $Ru^{\delta+}$ was present in the pristine perovskite matrix. After reduction, the Ru $3p_{3/2}$ of Ru NPs was deconvoluted into two peaks, which belonged to Ru^0 (461.6 eV) and $Ru^{\delta+}$ (463.17 eV), demonstrating that Ru NPs were exsolved from the perovskite lattice (Figure 2e).[32] In addition, the average valence state of Mn decreased slightly after exsolution (Figure 2f).[31]

Other than $LaMnO_3$, we also demonstrated that the noble-metal NPs could be also exsolved from other perovskite oxides. $LaFeO_3$ was selected as another host material for *in situ* exsolution of Ru and Ir NPs. HRTEM, XRD, and XPS results demonstrated that both Ir and Ru NPs can be successfully exsolved on the surface of $LaFeO_3$ perovskite matrix without the destruction of the perovskite structures (Figures S1 and S2).

https://doi.org/10.1021/acs.analchem.1c00721
Anal. Chem. 2021, 93, 5954−5962

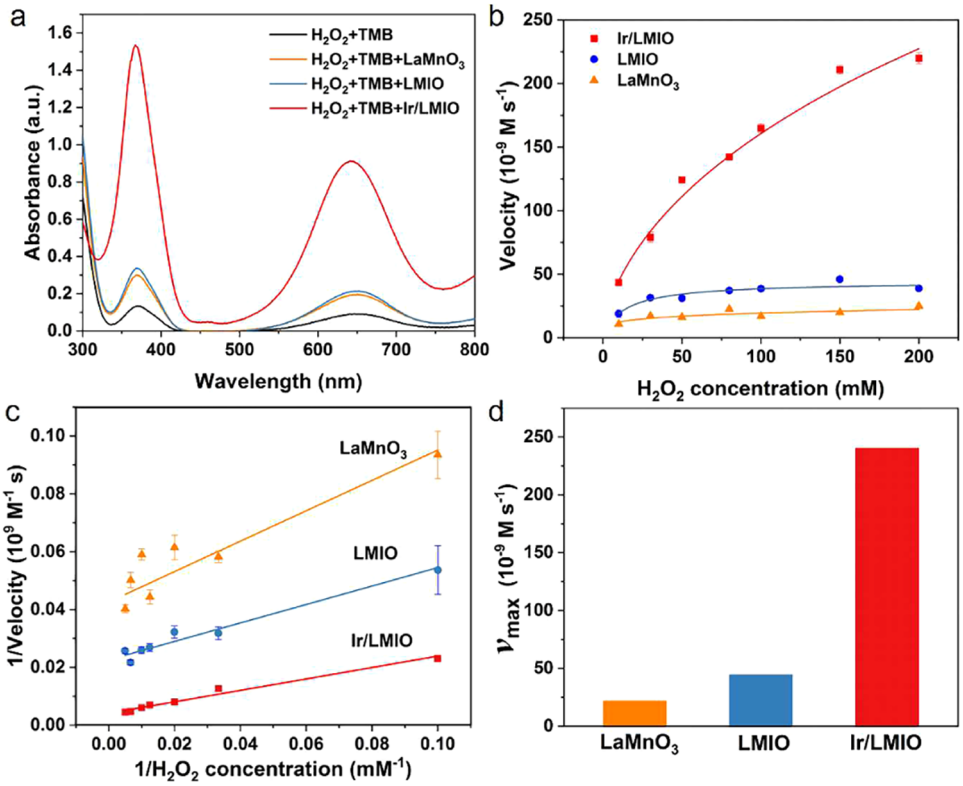

Figure 3. Peroxidase-like property of different nanozymes. (a) UV−vis spectra of samples containing 1 mM TMB, 20 mM H_2O_2, and 10 μg/mL of different nanozymes in 0.2 M acetate buffer for 10 min. (b) Plots of the velocity of the reaction versus different concentrations of H_2O_2 with 1 mM TMB and 10 μg/mL of different nanozymes in 0.2 M acetate buffer for 5 min. Error bars indicate standard deviations of three independent measurements. (c) Double-reciprocal plots of the velocity versus varying concentration of H_2O_2. Error bars indicate standard deviations of three independent measurements. (d) Comparison of the peroxidase-like activities through v_{max}.

Peroxidase-like Activity of Noble-Metal Nanoparticle/Perovskite Composites. After successful synthesis of Ir/LMIO, Ru/LMRO, Ir/LFIO, and Ru/LFRO, their peroxidase-like activities were evaluated by monitoring the catalytic oxidation of TMB in the presence of H_2O_2. As shown in Figure 3a, Ir/LMIO rapidly catalyzed the oxidation of TMB by H_2O_2, producing an obviously blue-colored oxidation product with a characteristic absorbance at 652 nm. However, the same concentration of H_2O_2 alone produced a negligible absorbance change. Moreover, in comparison to the parent $LaMnO_3$ and LMIO, Ir/LMIO had the highest catalytic efficiency of TMB oxidation in the presence of H_2O_2, indicating that *in situ* exsolution of Ir NPs on the surface of $LaMnO_3$ significantly enhanced the peroxidase-like activity of parental materials.

To investigate the kinetic process and quantify the peroxidase-like activity of noble NPs/perovskite composites after reduction, the steady-state kinetic measurements were performed. The kinetic data were obtained by changing the concentration of one substrate (e.g., H_2O_2 or TMB) when keeping the other's concentration constant. The enzyme kinetic parameters were obtained by Michaelis−Menten curves and the Lineweaver−Burk plot (Tables 1 and S1). Typical Michaelis−Menten curves of $LaMnO_3$, LMIO, and Ir/LMIO are shown in Figure 3b. The maximum initial velocity (v_{max}) and Michaelis−Menten constant (K_m) were obtained through the double-reciprocal plots of initial reaction rates (Figure 3c). The value of v_{max} showed the maximum rate as a critical indicator of the catalytic activity of the reaction. The value of K_m is inversely proportional to the affinity between the nanozymes and the substrate. It was noteworthy that,

Table 1. Comparisons of Kinetic Parameters between Different Peroxidase Mimics

substrate/H_2O_2	$LaMnO_3$	LMIO	Ir/LMIO	LMRO	Ru/LMRO
v_{max} (10^{-9} M s^{-1})	21.84	44.29	240.4	152.2	153.1
K_m (mM)	11.52	14.15	47.47	69.15	68.28
substrate/H_2O_2	$LaFeO_3$	LFIO	Ir/LFIO	LFRO	Ru/LFRO
v_{max} (10^{-9} M s^{-1})	2.699	3.468	139.0	7.819	82.24
K_m (mM)	32.45	14.42	52.33	27.46	93.58

compared to $LaMnO_3$ and LMIO, Ir/LMIO showed a much higher v_{max} value when H_2O_2 was used as the changing substrate (Figure 3d), indicating that the peroxidase-like activity of $LaMnO_3$ perovskite could be significantly enhanced by *in situ* exsolving Ir NPs. In addition, we also studied the kinetic parameters of LMRO, LFIO, and LFRO before and after exsolution. Typical Michaelis−Menten curves were obtained in the suitable concentration range of H_2O_2 (Figure 4a−c), which showed the same results as Ir/LMIO (i.e., after the exsolution, the peroxidase-like activities were enhanced). K_m and v_{max} values were obtained through the Lineweaver−Burk plot in Figure S3, which showed higher v_{max} values after exsolution (Figure 4d). We used the v_{max} value of the parent perovskites as the standard to normalize; the performance improvements of Ir/LMIO and Ru/LMRO are about 10 and 7 times higher than their parent material $LaMnO_3$, while the performance improvements of Ir/LFIO and Ru/LFRO are about 50 and 30 times higher than their parent material $LaFeO_3$, respectively. Among them, Ir/LMIO has the best

https://doi.org/10.1021/acs.analchem.1c00721
Anal. Chem. 2021, 93, 5954−5962

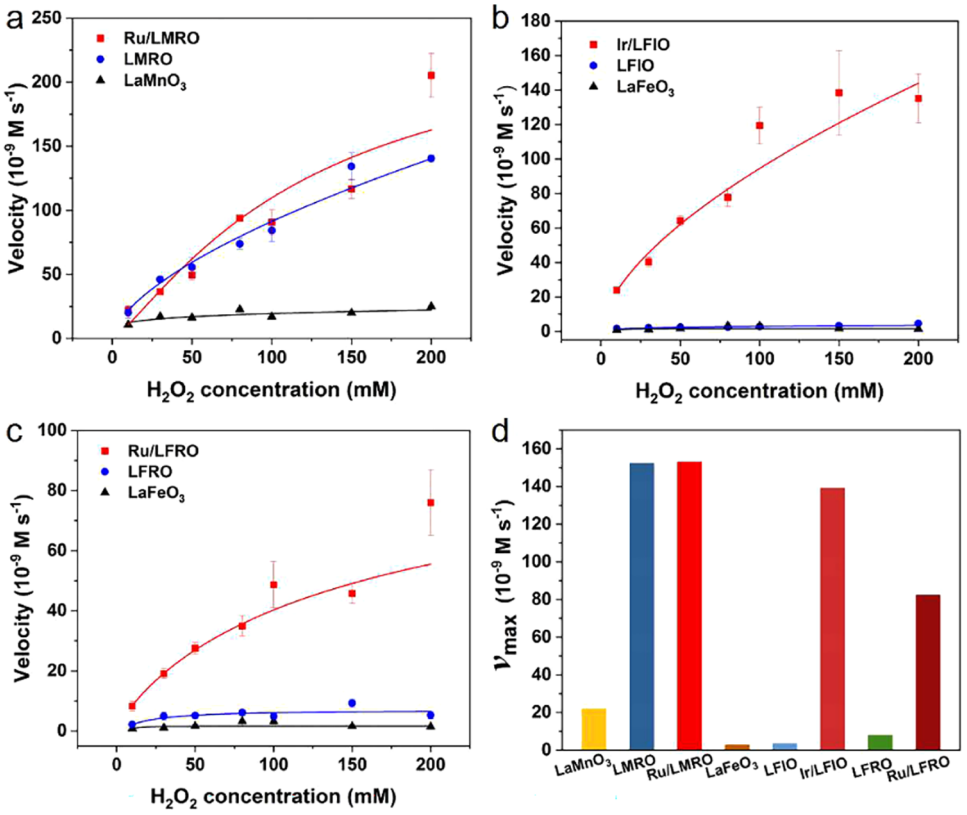

Figure 4. Steady-state kinetic assays of different nanozymes. Plots of the velocity of the reaction versus different concentrations of H_2O_2 with 1 mM TMB and 10 μg/mL different nanozymes in 0.2 M acetate buffer for 5 min. Error bars indicate standard deviations of three independent measurements. (a) Ru/LMRO, LMRO, and $LaMnO_3$. (b) Ir/LFIO, LFIO, and $LaFeO_3$. (c) Ru/LFRO, LFRO, and $LaFeO_3$. (d) Comparison of the peroxidase-like activities through v_{max}.

peroxidase-like activity due to the synergy between the highly catalytic activity of host perovskite and the noble-metal NPs.

The kinetic data with TMB as a substrate are presented in Figures S4 and S5 and Table S1, demonstrating that whether H_2O_2 or TMB as a substrate, the peroxidase-like activity of perovskite oxides was significantly improved after exsolution of Ir or Ru NPs.

In addition, Ir NPs with an average size of 2 nm were synthesized by a wet chemical method.[24] Both the catalytic efficiency and stability of free Ir NPs and incorporated ones were investigated. Our study demonstrated that the exsolution had little effect on the intrinsic catalytic activity of Ir NPs (Tables 1 and S1). However, after storing for more than 6 months, the peroxidase-like activity of Ir/LMIO was only reduced by 33%, while the activity of Ir NPs at the same mass concentration changed significantly with a 97% decrease (Figure S6). The above results demonstrated that *in situ* exsolution of noble-metal NPs from perovskite oxide surface can be a promising strategy that not only effectively improves the peroxidase-like activity of parental materials but also enhances the stability of noble-metal NPs.

Colorimetric Assay of ALP Activity. Alkaline phosphatase (ALP) is distributed at various levels in the body fluids and tissues of human, and its abnormal expression is closely related to many diseases. Therefore, it is significant to construct a colorimetric strategy to detect ALP with high sensitivity and selectivity in clinical diagnostics. ALP can catalyze the hydrolysis of the orthophosphoric monoesters (e.g., AAP) to produce ascorbic acid (AA).[38] As a kind of radical chain-breaker antioxidants, AA exhibits competitive effect on the reaction between H_2O_2 and TMB (Figure 5a). On the basis of this, we developed a colorimetric assay for ALP by coupling the cascade reactions of AAP hydrolysis and the nanozyme-catalyzed TMB oxidation (Figure 5a). As a proof of concept, we first investigated the inhibitory effect of AA on the TMB oxidation. As shown in Figures 5b and S7, the $A - A_0$ value decreased significantly with increasing AA concentration (where A and A_0 are the absorbances of the system at 652 nm after 5 min of the reaction and when the reaction just started, respectively). The linearity range for AA was 1−100 μM with a detection limit of 0.2 μM. Based on the above results, we performed experiments to assess the feasibility for detecting ALP activity. ALP or AAP exhibited a negligible effect on the TMB oxidation catalyzed by Ir/LMIO in the presence of H_2O_2 (Figure 5c). However, when ALP and AAP coexisted in the reaction system, the absorbance of oxTMB at 652 nm was substantially decreased because AAP was hydrolyzed to generate AA in the presence of ALP. As shown in Figure 5d, a good linear relationship between $A - A_0$ and ALP concentration was obtained. The linear range for ALP was 0.39−100 U/L, which was broader than most of other methods (Table S2). In addition, the limit of detection (LOD) of this sensing platform was as low as 0.39 U/L, demonstrating its potential for ALP detection in real serum samples. To demonstrate the unique advantages of Ir/LMIO, $LaMnO_3$ and LMIO were also used as peroxidase mimics for ALP detection. For comparison, the linear ranges of the LMIO/TMB/H_2O_2 and $LaMnO_3$/TMB/H_2O_2 sensing platforms were 0.24−8 and 0.34−10 U/L (Figures 5e and S8), respectively. The LODs were 0.24 and 0.34 U/L, respectively

https://doi.org/10.1021/acs.analchem.1c00721
Anal. Chem. 2021, 93, 5954−5962

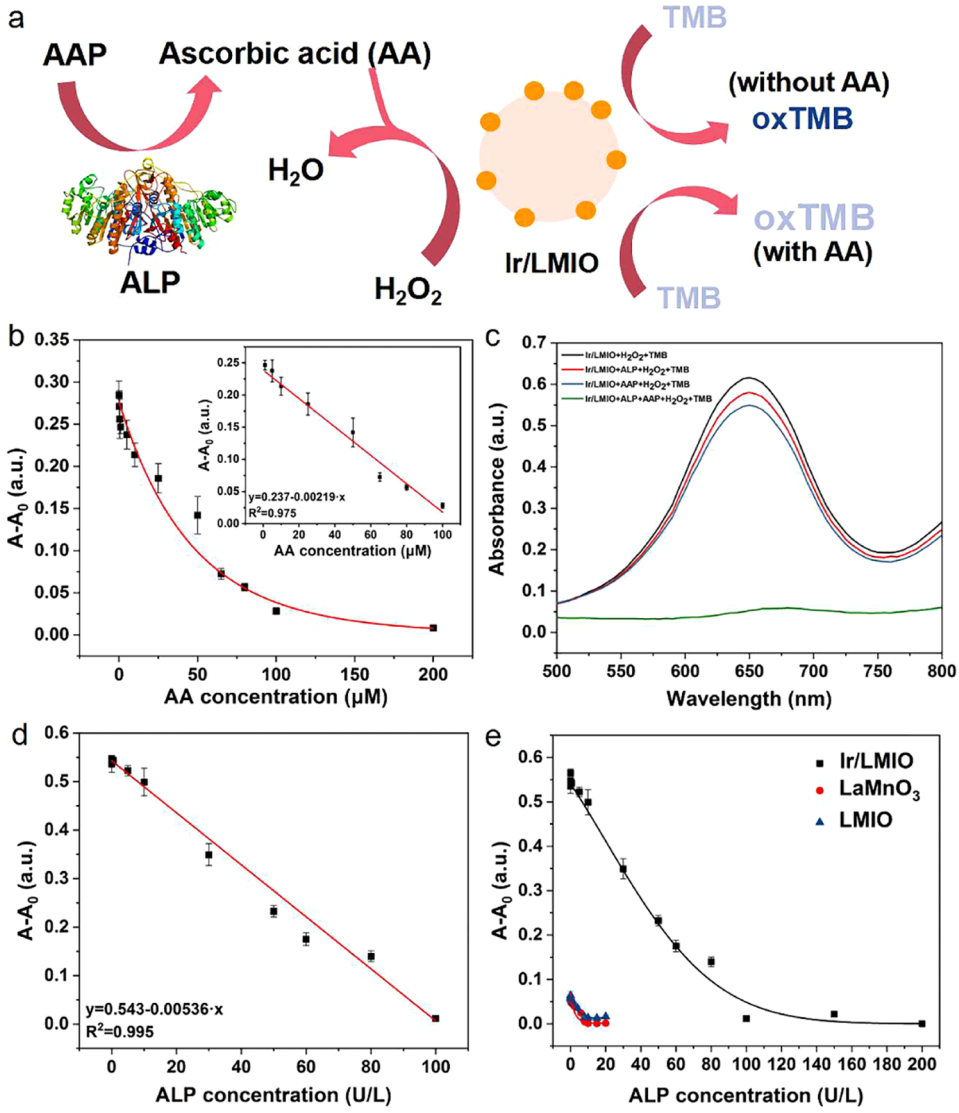

Figure 5. (a) Schematic illustration of a colorimetric platform for ALP activity assay. (b) Plot of $A - A_0$ versus concentrations of AA of Ir/LMIO. Inset: Linear plot of $A - A_0$ versus concentrations of AA. (c) UV−vis absorption spectra of various reaction systems. (d) Linear plot of $A - A_0$ versus concentrations of ALP (0.39−100 U/L). (e) Plot of $A - A_0$ versus concentrations of ALP of different nanozymes. Error bars indicate standard deviations of three independent measurements.

(Table S3). The substantially increased detection linear range for Ir/LMIO sensing platform could be mainly attributed to much higher peroxidase-like activity because other conditions of three sensing platforms were kept identical. The enhanced peroxidase-like activity of Ir/LMIO nanozyme makes the colorimetric system have greater application potential.

To evaluate the selectivity of the as-developed sensing method for ALP detection, we investigated possible interfering substances common in human serum. These include K^+, Na^+, Ca^{2+}, glucose oxidase (GOx), lysozyme, trypsin, lactate oxidase (LOx), HSA, BSA, fructose, glucose, glycine, glutamic acid, and sarcosine. Figure S9 shows that the interference of other substances on the sensing platform was negligible, confirming that the developed sensing system has a satisfactory selectivity toward ALP detection.

The ALP content in serum samples was measured to demonstrate the practical application of the colorimetric assay. As shown in Table 2, the recoveries for the four biological samples were between 95.20 and 102.60% with RSD less than 1.1%, suggesting that the proposed sensing system can accurately detect ALP in serum samples.

Table 2. Results for the Determination of ALP in Serum Samples

added (U/L)	found (U/L)	recovery (%)	RSD (%, n = 3)
10	10.26	102.60	1.09
7.5	7.54	100.51	0.21
5	5.00	100	0.54
2.5	2.38	95.20	1.02

CONCLUSIONS

In conclusion, a general and effective *in situ* exsolution strategy was developed to prepare highly active peroxidase-like nanozymes. The *in situ* exsolution of Ir or Ru NPs from noble-metal-substituted A-site-deficient perovskites can not only effectively improve the peroxidase-like activity of parent perovskite but also improve the stability of noble-metal NPs. The obtained Ir/LMIO nanozyme has the highest peroxidase-

https://doi.org/10.1021/acs.analchem.1c00721
Anal. Chem. 2021, 93, 5954−5962

like activity compared with other exsolved nanozymes. Through coupling Ir/LMIO nanozyme with ascorbic acid 2-phosphate, a facile colorimetric assay for ALP activity detection with high sensitivity and selectivity was developed. This study not only provides a promising strategy to rationally design nanomaterials with peroxidase-mimicking activity but also develops a facile colorimetric assay to sensitively detect ALP activity.

■ ASSOCIATED CONTENT

Supporting Information

The Supporting Information is available free of charge at https://pubs.acs.org/doi/10.1021/acs.analchem.1c00721.

TEM images, PXRD patterns, XPS survey scans, kinetic curves, absorption spectra, stability of free Ir NPs and Ir/LMIO, comparisons of kinetic parameters between different peroxidase mimics, and comparisons of analytical performance between different peroxidase mimics of this work in ALP detection (PDF)

■ AUTHOR INFORMATION

Corresponding Author

Hui Wei − *Department of Biomedical Engineering, College of Engineering and Applied Sciences, Nanjing National Laboratory of Microstructures, Jiangsu Key Laboratory of Artificial Functional Materials, Nanjing University, Nanjing, Jiangsu 210023, China; State Key Laboratory of Analytical Chemistry for Life Science, School of Chemistry and Chemical Engineering, Chemistry and Biomedicine Innovation Center (ChemBIC), Nanjing University, Nanjing, Jiangsu 210023, China; Key Laboratory of Analytical Chemistry for Biology and Medicine (Ministry of Education), Wuhan University, Wuhan 430072, China;* orcid.org/0000-0003-0870-7142; Phone: +86-25-89683272; Email: weihui@nju.edu.cn; Fax: +86-25-89684648; http://weilab.nju.edu.cn/

Authors

Xiaoqian Jiang − *Department of Biomedical Engineering, College of Engineering and Applied Sciences, Nanjing National Laboratory of Microstructures, Jiangsu Key Laboratory of Artificial Functional Materials, Nanjing University, Nanjing, Jiangsu 210023, China*

Xiaoyu Wang − *Department of Biomedical Engineering, College of Engineering and Applied Sciences, Nanjing National Laboratory of Microstructures, Jiangsu Key Laboratory of Artificial Functional Materials, Nanjing University, Nanjing, Jiangsu 210023, China;* orcid.org/0000-0002-8641-2430

Anqi Lin − *Department of Biomedical Engineering, College of Engineering and Applied Sciences, Nanjing National Laboratory of Microstructures, Jiangsu Key Laboratory of Artificial Functional Materials, Nanjing University, Nanjing, Jiangsu 210023, China*

Complete contact information is available at: https://pubs.acs.org/10.1021/acs.analchem.1c00721

Author Contributions

‖X.J. and X.W. contributed equally to this work. The manuscript was written through contributions of all authors. All authors have given approval to the final version of the manuscript.

Notes

The authors declare no competing financial interest.

■ ACKNOWLEDGMENTS

This work was supported by the National Key R&D Program of China (2019YFA0709200), National Natural Science Foundation of China (21874067 and 21722503), the China Postdoctoral Science Foundation (2019TQ0144 and 2019M661786), CAS Interdisciplinary Innovation Team (JCTD-2020-08), PAPD Program, Open Funds of Key Laboratory of Analytical Chemistry for Biology and Medicine (Wuhan University), Ministry of Education (ACBM2019001), the Innovation Foundation of Nanjing University, and Fundamental Research Funds for the Central Universities (021314380145).

■ REFERENCES

(1) Wei, H.; Wang, E. *Chem. Soc. Rev.* **2013**, *42*, 6060−6093.
(2) Wu, J.; Wang, X.; Wang, Q.; Lou, Z.; Li, S.; Zhu, Y.; Qin, L.; Wei, H. *Chem. Soc. Rev.* **2019**, *48*, 1004−1076.
(3) Tonga, G. Y.; Jeong, Y. D.; Duncan, B.; Mizuhara, T.; Mout, R.; Das, R.; Kim, S. T.; Yeh, Y. C.; Yan, B.; Hou, S.; Rotello, V. M. *Nat. Chem.* **2015**, *7*, 597−603.
(4) Huang, M.; Wang, H.; He, D.; Jiang, P.; Zhang, Y. *Chem. Commun.* **2019**, *55*, 3634−3637.
(5) Zhang, Z.; Zhang, X.; Liu, B.; Liu, J. *J. Am. Chem. Soc.* **2017**, *139*, 5412−5419.
(6) Liang, X.; Han, L. *Adv. Funct. Mater.* **2020**, *30*, No. 2001933.
(7) Huang, L.; Chen, J. X.; Gan, L. F.; Wang, J.; Dong, S. J. *Sci. Adv.* **2019**, *5*, No. eaav5490.
(8) Liu, X.; Huang, D.; Lai, C.; Qin, L.; Zeng, G.; Xu, P.; Li, B.; Yi, H.; Zhang, M. *Small* **2019**, *15*, No. 1900133.
(9) Ge, C.; Wu, R.; Chong, Y.; Fang, G.; Jiang, X.; Pan, Y.; Chen, C.; Yin, J.-J. *Adv. Funct. Mater.* **2018**, *28*, No. 1801484.
(10) Gao, L.; Zhang, Y.; Zhao, L. N.; Niu, W. C.; Tang, Y. H.; Gao, F. P.; Cai, P. J.; Yuan, Q.; Wang, X. Y.; Jiang, H. D.; Gao, X. Y. *Sci. Adv.* **2020**, *6*, No. eabb1421.
(11) Xu, B. L.; Wang, H.; Wang, W. W.; Gao, L. Z.; Li, S. S.; Pan, X. T.; Wang, H. Y.; Yang, H. L.; Meng, X. Q.; Wu, Q. W.; Zheng, L. R.; Chen, S. M.; Shi, X. H.; Fan, K. L.; Yan, X. Y.; Liu, H. Y. *Angew. Chem., Int. Ed.* **2019**, *58*, 4911−4916.
(12) Zhang, L.; Liu, Z.; Deng, Q.; Sang, Y.; Dong, K.; Ren, J.; Qu, X. *Angew. Chem., Int. Ed.* **2020**, *132*, 1−7.
(13) Kim, M. S.; Lee, J.; Kim, H. S.; Cho, A.; Shim, K. H.; Le, T. N.; An, S. S. A.; Han, J. W.; Kim, M. I.; Lee, J. *Adv. Funct. Mater.* **2020**, *30*, No. 1905410.
(14) Gao, L.; Zhuang, J.; Nie, L.; Zhang, J.; Zhang, Y.; Gu, N.; Wang, T.; Feng, J.; Yang, D.; Perrett, S.; Yan, X. *Nat. Nanotechnol.* **2007**, *2*, 577−583.
(15) Ling, P.; Zhang, Q.; Cao, T.; Gao, F. *Angew. Chem., Int. Ed.* **2018**, *57*, 6819−6824.
(16) Han, L.; Zhang, H.; Chen, D.; Li, F. *Adv. Funct. Mater.* **2018**, *28*, No. 1800018.
(17) Jin, C.; Lian, J.; Gao, Y.; Guo, K.; Wu, K.; Gao, L.; Zhang, X.; Zhang, X.; Liu, Q. *ACS Sustainable Chem. Eng.* **2019**, *7*, 13989−13998.
(18) Feng, L. L.; Liu, B.; Xie, R.; Wang, D. D.; Qian, C.; Zhou, W. Q.; Liu, J. W.; Jana, D.; Yang, P. P.; Zhao, Y. L. *Adv. Funct. Mater.* **2020**, No. 2006216.
(19) Wang, X.; Gao, X. J.; Qin, L.; Wang, C.; Song, L.; Zhou, Y.-N.; Zhu, G.; Cao, W.; Lin, S.; Zhou, L.; Wang, K.; Zhang, H.; Jin, Z.; Wang, P.; Gao, X.; Wei, H. *Nat. Commun.* **2019**, *10*, No. 704.
(20) Suntivich, J.; Gasteiger, H. A.; Yabuuchi, N.; Nakanishi, H.; Goodenough, J. B.; Shao-Horn, Y. *Nat. Chem.* **2011**, *3*, 546−550.
(21) Song, L.; Zhu, Y.; Yang, Z.; Wang, C.; Lu, X. *J. Mater. Chem. B* **2018**, *6*, 5931−5939.

(22) Wang, X.; Cao, W.; Qin, L.; Lin, T.; Chen, W.; Lin, S.; Yao, J.; Zhao, X.; Zhou, M.; Hang, C.; Wei, H. *Theranostics* **2017**, *7*, 2277−2286.
(23) Xia, X.; Zhang, J.; Lu, N.; Kim, M. J.; Ghale, K.; Xu, Y.; McKenzie, E.; Liu, J.; Yet, H. *ACS Nano* **2015**, *9*, 9994−10004.
(24) Wang, X.; Qin, L.; Zhou, M.; Lou, Z.; Wei, H. *Anal. Chem.* **2018**, *90*, 11696−11702.
(25) Su, H.; Liu, D. D.; Zhao, M.; Hu, W. L.; Xue, S. S.; Cao, Q.; Le, X. Y.; Ji, L. N.; Mao, Z. W. *ACS Appl. Mater. Interfaces* **2015**, *7*, 8233−8242.
(26) Kwon, O.; Sengodan, S.; Kim, K.; Kim, G.; Jeong, H. Y.; Shin, J.; Ju, Y.-W.; Han, J. W.; Kim, G. *Nat. Commun.* **2017**, *8*, No. 15967.
(27) Neagu, D.; Papaioannou, E. I.; Ramli, W. K. W.; Miller, D. N.; Murdoch, B. J.; Menard, H.; Umar, A.; Barlow, A. J.; Cumpson, P. J.; Irvine, J. T. S.; Metcalfe, I. S. *Nat. Commun.* **2017**, *8*, No. 1855.
(28) Wu, Q.; Yan, B.; Cen, J.; Timoshenko, J.; Zakharov, D. N.; Chen, X.; Xin, H. L.; Yao, S.; Parise, J. B.; Frenkel, A. I.; Stach, E. A.; Chen, J. G.; Orlov, A. *Chem. Mater.* **2018**, *30*, 1585−1592.
(29) van Deelen, T. W.; Mejia, C. H.; de Jong, K. P. *Nat. Catal.* **2019**, *2*, 955−970.
(30) Neagu, D.; Tsekouras, G.; Miller, D. N.; Menard, H.; Irvine, J. T. S. *Nat. Chem.* **2013**, *5*, 916−923.
(31) Gao, Y.; Wang, J.; Lyu, Y.-Q.; Lam, K.; Ciucci, F. *J. Mater. Chem. A* **2017**, *5*, 6399−6404.
(32) Jiang, Y.; Geng, Z.; Yuan, L.; Sun, Y.; Cong, Y.; Huang, K.; Wang, L.; Zhang, W. *ACS Sustainable Chem. Eng.* **2018**, *6*, 11999−12005.
(33) Zhang, J. W.; Gao, M. R.; Luo, J. L. *Chem. Mater.* **2020**, *32*, 5424−5441.
(34) Zheng, F.; Guo, S.; Zeng, F.; Li, J.; Wu, S. *Anal. Chem.* **2014**, *86*, 9873−9879.
(35) Chen, C. X.; Zhao, D.; Jiang, Y. Y.; Ni, P. J.; Zhang, C. H.; Wang, B.; Yang, F.; Lu, Y. Z.; Sun, J. *Anal. Chem.* **2019**, *91*, 15017−15024.
(36) Lee, J.; Bubar, C. T.; Moon, H. G.; Kim, J.; Busnaina, A.; Lee, H.; Shefelbine, S. J. *ACS Sens.* **2018**, *3*, 2709−2715.
(37) Gao, Z. Q.; Deng, K. C.; Wang, X. D.; Miro, M.; Tang, D. P. *ACS Appl. Mater. Interfaces* **2014**, *6*, 18243−18250.
(38) Peng, C.; Xing, H. H.; Xue, Y.; Wang, J.; Li, J.; Wang, E. K. *Nanoscale* **2020**, *12*, 2022−2027.
(39) Li, Y.; Zhang, W.; Zheng, Y.; Chen, J.; Yu, B.; Chen, Y.; Liu, M. *Chem. Soc. Rev.* **2017**, *46*, 6345−6378.
(40) Cali, E.; Kerherve, G.; Naufal, F.; Kousi, K.; Neagu, D.; Papaioannou, E. I.; Thomas, M. P.; Guiton, B. S.; Metcalfe, I. S.; Irvine, J. T. S.; Payne, D. J. *ACS Appl. Mater. Interfaces* **2020**, *12*, 37444−37453.

https://doi.org/10.1021/acs.analchem.1c00721
Anal. Chem. 2021, 93, 5954−5962